Military Technical College
Kobry El-Kobbah,
Cairo, Egypt

8th International Conferenc
on
Chemical & Environmenta
Engineering
19 – 21 April 2016

TANM -4
Novel (3D, 1D and 2D) of WO$_3$/TiO$_2$NT–graphene ternary nanocomposites for high efficiency visible light photocatalysis

Heba H. El-Maghrabi[1] and Yasser M. Moustafa[1]

Abstract

Due to the increasing need to environment protection in real time need to energize new materials are under extensive investigations. Between others, TiO$_2$ nanotubes (TNTs), graphene sheets and WO$_3$ NPs as 1D, 2D and 3D materials are promising alternatives as high efficiency visible light photocatalyst due to their unique properties and their superior charge transport properties. Our efforts in this domain aim the construction of new ternary nanocomposite of WO$_3$/TiO$_2$NT–graphene. The structure, surface morphology, chemical composition and optical properties were characterized by X-ray diffraction (XRD), Raman, Fourier-transform infrared spectroscopy (FT-IR), scanning electron microscopy (SEM), energy dispersive X-ray spectrometer (EDS), transmission electron microscopy (TEM), selected area electron diffraction (SAED) and UV–vis diffuse reflectance spectroscopy (DRS). XRD results confirm the interaction of TiO$_2$-NT with graphene. This novel composite shows remarkably enhanced performance for phenol compounds photodegradation. The high photocatalytic activity of the nanocomposite is found to be related to the increased adsorption toward chemical species, enhanced light absorption and efficient charge separation and transfer.

Keywords:
Graphene, Titanium dioxide nanotubes, green chemistry, photocatalyst

----
[1]Egyptian Petroleum Research Institute, 11727, Cairo, Egypt

Military Technical College
Kobry El-Kobbah,
Cairo, Egypt

8ᵗʰ International Conferenc
on
Chemical & Environmenta
Engineering
19 – 21 April 2016

l. Introduction

Recently, the nanostructures are classified based on their morphology and their efficiency is considered with respect to the influencing parameters. We suggest effective ways of engineering catalyst combinations to overcome the current performance barriers. graphene-based composites have received considerable attention due to their potential application in the photocatalytic field [1–4]. It is now understood that, graphene-based composites exhibit higher photocatalytic property because graphene has perfect two-dimensional carbon structure with better conductivity and larger surface area [1].

In general, graphene-based composites are prepared from the reduction of graphene oxide (GO)-based composites through the chemical reduction method, the flash reduction method or the solvothermal method, etc. However, green formation of GO-based composites has recently proven to be an effective method to produce graphene-based composites [5-7]. One-, two- and three-dimensional nanostructures in both pristine and modified forms have shown great potential as catalysts in photocatalysis. The development for efficient photocatalysts with visible light response has become are search focus in the photocatalytic field [8-10]. As a visible-light-driven semiconductor, tungsten oxide (WO_3) as 3D nanoparticles and titanium dioxide (TiO_2) as 1D nanotubes have attracted considerable attention in recent years owing to its strong adsorption in visible light spectrum and promising physicochemical properties [11-12]. In our previous work TiO_2NT–graphene nanocomposites were synthesized [13]. this work, WO_3/TiO_2NT–graphene ternary nanocomposites were synthesized as 1D, 2D and 3D system for high efficiency visible light phenol compounds photodegradation.

2. Experimental

2.1. Preparation of graphene oxide (GO)

GO was prepared by oxidizing the graphite powder in a mixture of concentrated sulphuric acid, $NaNO_3$ and $KMnO_4$ according to modified Hummers method [14]. Briefly, graphite powder was stirred in 98% H_2SO_4 and $NaNO_3$ on a magnetic stirrer for 2 h. Then $KMnO_4$ was gradually added into the above solution by maintaining the temperature less than 20 °C. The mixture was then stirred at 35 °C for 2 h in an oil-bath. The resulting solution was diluted by adding double distilled water under vigorous stirring for 1 h. Then a dark brown suspension was obtained. The suspension was further treated by adding 30 % H_2O_2 solution drop wise until the color of the solution became bright yellow. The resulting GO suspension was washed by repeated centrifugation, first with 5 % aqueous HCI solution to remove excess of manganese salt followed by double distilled water until the pH of the solution became near neutral. The purified GO was finally dispersed in double distilled water ultrasonically to obtain a stable dispersion of GO Figure (1).

2.2. Preparation of TiO₂ nanotubes (TiO₂NT)

TiO_2NT were prepared by the modified hydrothermal method [15]. In a typical run, 2 g TiO_2 added into 50 mL of different concentration of NaOH aqueous solution and the suspension system was stirred for 1 hour at room temperature to form a suspension. Then, the mixture was transferred to a Teflon-lined stainless steel autoclave. The autoclave was heated statically at different temperature and different duration time. After cooled naturally in air, the mixture was centrifuged at a speed of 4000 rpm and. The precipitates were collected. The white powder was thoroughly washed with different concentration of HCI aqueous solution then drying at 80 °C. All prepared samples were calcinated for 4 hours at different temperature Figure (2).

2.3. Green preparation of binary TiO₂NT-graphene nanocomposites

TiO_2NT-graphene nanocomposite samples were prepared by a simple one-pot. In brief, titania powders were mixed with ultrasonically dispersed GO in aqueous solution of Ascorbic acid for 2 h, then the solution was subjected to stirring for 24h at room temperature. The resulting nanocomposite was collected by centrifugation and washed with double distilled H_2O followed by drying at 50 °C for 2 days. After that, the solid was collected. The synthetic route of TG is shown in Figure (3).

2.4. Preparation of WO₃ nanoparticles

The preparation of WO_3 nanoparticles will be done by using chelation-polymerization technique (Pechini method) **[16]** ethylene glycol aqueous solution (EG, >99%) has desired concentration was added, first, to an aqueous solution of citric acid (CA, 99.5%) to carry out the esterification under constant stirring and heated at 60°C for 30 min.
Secondly, the ester was heated to 80°C with stirring, then 500, 0.1 M metal solution (ammonium metatungstate precursors (>99.5%)) was added during the stirring for another 30 min, accordingly tungstic acids was created and consequently the pH of the medium decreased to the value of 1.4. In the third step, the solutions were microwave 900 W to complete removal of water (25 min), yielding solid resins. The resulted resins were ground in an agate mortar and suffered to a calcination process at 500°C for 4h in presence of purified air.

2.5 Preparation of WO₃/TiO₂NT–graphene ternary nanocomposites

In a typical procedure, the prepared TiO_2NT–graphene was dispersed in double distilled water to form a homogeneous solution was mixed with WO_3 solution and sonicated for 2 h at room temperature then heated to 70 °C. Different content of WO_3 in WTG-x (x: 10, 20 and 30 wt%, respectively) were also obtained to investigate the effect of WO_3 loading.

Military Technical College
Kobry El-Kobbah,
Cairo, Egypt

8th International Conferenc
on
Chemical & Environmenta
Engineering
19 – 21 April 2016

2.6. Characterization

Fourier-transform infrared spectroscopy (FT-IR) spectrum of sample was recorded between 4000 and 500 cm^{-1} with an FTIR spectrometer Perkin Elmer (model spectrum one FT-IR spectrometer, USA). Samples were prepared using the standard KBr pellets. The phase of the powers was identified by an X-ray diffractometer (XRD, Shimadzu XD-l) with a Cu Ka radiation at 40 kV and 30 mA over the 2θ range of 4-80° at a scanning speed of 4°/ min with a sampling angle interval of 0.04°. Raman test was carried out using the dispersive Raman microscope (Model Sentera, Bruker, Germany) instrument at laser wave length 532 nm [doubled Nd:YAG laser (neodymium-doped ytrium aluminum garnet)] and power l0 mW . UV-vis diffuse reflectance spectroscopy (UV-vis DRS) was carried out on Jasco model V-570A. Transmission electron microscopy and Selected area electron diffraction (SAED) was performed on JEOL JEM 2100 were used to characterize the crystallites size and shape of the photocatalysts.

2.7. Photocatalytic activity

Photocatalytic reactions were conducted in a commercial photo-reactor equipped with a 500 ml cylindrical Pyrex vessel irradiated directly with solar irradiated. For photocatalytic phenol degradation, 0.2 g of the catalyst was mixed with 500 ml of 50mg/l phenol solution which was further stirred in the dark for 60 min to reach the adsorption equilibrium prior to the photocatalytic test. During the photocatalytic reaction, samples were collected at selected time intervals and the catalyst particles were removed by centrifugation. The residual phenol concentration was determined using HPLC (Agilent 1200, USA), equipped with an ultraviolet (UV) detector and a C18 reversed phase column (250mm×4.5mm, Agilent, USA) at 30 ℃. The mobile phase consists of water and acetonitrile (40/60, v/v) with a flow rate of 1.0 ml min^{-1}.

3. Results and discussion

3.1. Characterization of the photocatalysts

The XRD patterns of pure WO_3 and WO_3/TiO_2NT–graphene (WTGs) ternary nanocomposites are shown in **Figure (4)**, all the peaks can be indexed to the hexagonal phase of WO_3 (JCPDS no. 75-2187) with well resolved (002), (020), (200), (112), (022), (202) and (222) reflections. X-ray diffraction (XRD) patterns between 22° ~ 25° of pure WO_3 have three well defined peaks at 2θ = 23.12°, 23.59° and 24.38°, corresponding to (002), (020) and (200) diffractions of monoclinic crystal structure with d spacing 0.385, 0.377 and 0.365 nm or interlayer spacing 0.77, 0.76 and 0.73 nm respectively.
For the WTGs ternary nanocomposites, no typical peaks belonging to graphene and TiO_2NT are observed besides these representative diffraction peaks of WO_3. It can be ascribed to the low amount and low diffraction intensity of graphene, compared to the characteristic peaks of

Military Technical College
Kobry El-Kobbah,
Cairo, Egypt

8th International Conferenc
on
Chemical & Environmenta
Engineering
19 – 21 April 2016

WO$_3$ between 20 and 30 º indicating the crystalline WO$_3$ formed on the surface of TiO$_2$NT–graphene nanocomposite.

Depicts the FTIR spectra of pure WO$_3$ and WTGs ternary nanocomposites are observed at Figure (5) The peak at about 3420 cm^{-1} in the spectra corresponds to the stretching vibration mode of –OH and the physically adsorbed H$_2$O also contributes to this peak. The peaks at 1326 and 1643 cm^{-1} are attributed to the W-O stretching and O–H bending vibration, respectively. As for pure WO$_3$, the two broad absorption bands appear at 807 and 748 cm^{-1} owing to the vibration of W–O–W bond. In another words the broad IR bands of WO$_3$ in nano-materials are observed at 748 cm^{-1} (W–O bending modes) and 807 cm^{-1} (W–O stretching modes) identifying the crystalline WO$_3$. While the FTIR spectra of WTGs have the absorption at 919, 704 and 472 cm^{-1} is assigned to the Ti–O–Ti vibration.

Raman spectra of pure WO$_3$ and WO$_3$/TiO$_2$NT–graphene (WTGs) ternary nanocomposites are shown in Figure (6), the octahedral systems of WO$_3$ have WO$_3$ stretching and bending vibrations occur invariably in the 950-600 and 400-200 cm^{-1} regions, respectively, with subclassifications for the short terminal W=O bonds and the bridging W-O-W bonds. Bending vibration modes of O–W–O are shown at 261 cm^{-1} and 327 cm^{-1} and stretching vibration modes of O–W–O are shown at 807 cm^{-1} and 763 cm^{-1}. In order to confirm the formation of WTGs ternary nanocomposites, the Raman peaks of G in TGs hybrids were examined in the range from 1000 to 2000 cm^{-1}. The Raman peaks were observed at 1352 cm^{-1} and at 1574 cm^{-1} corresponding to D- and G-bands of G, respectively, indicating the successful formation of WO$_3$ nanoparticles on 3D TGs surfaces. Small I_D/I_G peak intensity ratio (I_D/I_G = 1.10) compared to the pristine RGO (I_D/I_G = 1.23) of Raman spectra indicates lower defects and disorders of RGO in WTGs ternary nanocomposites. The peaks located at about 148, 397, 516 and 635 cm^{-1}, which are corresponding to E_g, B_{1g}, B_{1g} or A_{1g}, E_g modes of anatase phase cannot be seen, which may be due to that the region of anatase phase disguises the stretching and bending vibrations area of WO$_3$.

The morphologies of the pure WO$_3$ and WO$_3$/TiO$_2$NT–graphene ternary nanocomposites with different concentrations of graphene are observed by HR-TEM images. As shown in Figure (7), a small WO$_3$ nanoparticles with a diameter of 6 nm are uniform distribution on the surface of graphene after the reaction. Indicates the existence of much larger agglomerated structures in WTG-20 corresponding to increase of WO$_3$ ratio. When one side of the TiO$_2$ nanotubes bonds to the spherical WO$_3$ nanoparticles surface, it distorts the graphene structure, leading to the increased interlayer spacing. As the distribution would cause somewhat irregularity. The spacing between adjacent layers is ~0.7–1.2 nm. As it is significantly larger than the layer spacing in the standard graphene structure. Figure (8) shows selected area electron diffraction (SAED) patterns of the pure WO$_{3(6nm)}$ and WTGs ternary nanocomposites. The former can be indexed to face-centered- monoclinic crystal structure of WO$_3$ NPs.

Military Technical College
Kobry El-Kobbah,
Cairo, Egypt

8ᵗʰ International Conferenc
on
Chemical & Environmenta
Engineering
19 – 21 April 2016

The elemental composition of the WTGs nanocomposites are determined by energy-dispersive X-ray (EDX) spectroscopy experiment, as is supplied in Figure (9). As a result, C, O, Ti and W elements were identified as shown in Table 1.

Table 1: The atomic ratio composition of the WTGs nanocomposites.

Element	WTG-5	WTG-10	WTG-20
W	2.12	7.99	13.98
C	25.58	23.99	21.57
O	27.71	26.18	26.83
Ti	44.59	41.84	37.62

The UV–vis diffuse reflectance spectra of the pure WO_3, and WO_3/TiO_2NT–graphene nanocomposites with various WO_3 contents from 5 to 20 wt% were shown in Figure (10). It can be observed that all spectra exhibit a characteristic absorption band around 460 nm, indicating the existence of highly crystallized WO_3. The spectrum of WTG-5 has relatively lower absorption intensity in the visible region compared with WTG-20 nanocomposites. The absorption of WTGs nanocomposites in the visible region increases along with the content of WO_3 increasing in the preparation process. Moreover, due to the restoration of the π–πconjugation network of RGO in the nanocomposite, the absorption band-edges show a continuous red-shift along with increasing WO_3 content. The band gap of WTGs nanocomposites has been determined in Table 2. The reduction of band gap could be attributed to the interaction between WO_3 and RGO.

Table 2: The band gap energy of WTGs nanocomposites.

Samples	WTG-5	WTG-10	WTG-20
Eg (ev)	2.2	2.1	1.9

3.2. Catalytic activity of prepared WTGs ternary nanocomposites

Phenol photodegradation over WTGs ternary nanocomposites samples as a function of solar irradiation time are shown in Figure (11). Attributed to its reduced band-gap, the degradation of the phenol under solar irradiation by using the WTGs is very high. Based on comparing the photo catalytic performances of the TiO_2NT–graphene of TG-10, TG-20 and TG-30 it can be inferred that chemical bond between the graphene and WO_3 is the precondition for the visible-light activity. It is not surprising to the excess WO_3 (20 wt%) on WTG-20 has highest activity. Moreover, the absorbability of these materials was analysed in dark, and the results are shown in Figure (11). The great absorbability of the TiO_2NT–graphene results from its large surface area. Therefore, the graphene really acts as a sensitizer in the photocatalyst.

Military Technical College
Kobry El-Kobbah,
Cairo, Egypt

8th International Conference
on
Chemical & Environmental
Engineering
19 – 21 April 2016

The photocatalytic mechanism of the WTGs nanocomposites is suggested as follows: It is known that oxygen vacancies in WO_3 lattice structure act as electron donors to provide electrons to its conduction band, making WO_3 an n-type semiconductor and the TG/WO_3 interface a Schottky junction, as illustrated in Figure (12). As the work function of n-type WO_3 is smaller than that of TG, electrons transfer from WO_3 to TG in the surface, leading to negatively charged surface produces negatively charged oxygen species such as $O^{\delta-}$, $O_2^{\delta-}$, etc. on its surface under visible-light irradiation which is in favor of utilizing efficiency of photogenerated electrons and high photoactivity. These electrons transferred to the surface of WTGs and reacted with oxygen to yield superoxide and hydroxyl radicals.

4. Conclusion

The incorporation of WO_3 nanoparticles with TiO_2NT–graphene for high efficiency photocatalytic application were prepared from TiO_2NT and GO by a simple green process. The obtained photocatalysts were characterized by Raman, FT-IR, XRD, EDS and TEM. The influences of GO content were investigated by measuring the photocatalytic performance for the degradation of phenol under solar irradiation. The degradation efficiency of phenol could be obtained 94 % at a GO content of 20% within 180 min. The high photocatalytic activity of TGs is attributed to the decrease in band gap values increasing with the amount of graphene, for which graphene can slow the electron–hole pairs, increase charge transfer rate of electrons, and increase surface-adsorbed amount of chemical molecules through π–π interactions. The obtained results indicated that the prepared WO_3/TiO_2NT–graphene nanocomposites photocatalyst has a potential application for the industrial effluents wastewater treatment containing phenol.

5. References

[1]   Liu JC, Bai HW, Wang YJ, Liu ZY, Zhang XW, Sun DL. Adv Funct Mater 2010; 20:4175–81.
[2]   Ying H, Wang ZY, Guo ZD, Shi ZJ, Yang SF. Acta Phys Chim Sin 2011; 27:1482–6.
[3]   Wang F, Zhang K, Mol J. Catal A Chem 2011; 345:101–7.
[4]   Li Q, Guo BD, Yu JG, Ran JR, Zhang BH, Yan HJ, et al. J Am Chem Soc 2011;133:10878–84.
[5]   Qin JW, Cao MH, Li N, Hu CW. J Mater Chem 2011;21:17167–74.
[6]   Wu TS, Liu S, Luo YL, Lu WB, Wang L, Sun XP. Nanoscale 2011; 3:2142–4.
[7]   Chandra V, Park J, Chun Y, Lee JW, Hwang IC, Kim KS. ACS Nano 2010;4: 3979–86.
[8]   TongH, OuyangSX, BiYP, UmezawaN, OshikiriM, YeJH.AdvMater 2012; 24:229–51.
[9]   Hernández-AlonsoMD, FresnoF, SuárezS, CoronadoJM. EnergyEnvironSci 2009; 2:1231–57.
[10] KubackaA, Fernández-GarcíaM, ColónG.ChemRev2012; 112:1555–614.
[11] YuJG, QiLF.JHazardMater2009; 169:221–7.
[12] PengTY, KeDN, XiaoJR, WangL, HuJ, ZanL.JSolidStateChem 2012; 194:250–6.

Military Technical College
Kobry El-Kobbah,
Cairo, Egypt

8th International Conferenc
on
Chemical & Environmenta
Engineering
19 – 21 April 2016

[13] HuangJR, XuXJ, GuCP, FuGJ, WangWZ, LiuJH.MaterResBull 2012; 47:3224–32.
[14] Hummers, William S.; Offeman, Richard E., Journal of the American Chemical Society 80. 6 (March 20, 1958) 1339.
[15] Nan Liu, Xiaoyin Chen, Jinli Zhang, Johannes W. Schwanka, Catalysis Today 225 (2014) 34– 51.
[16] T. Zaki, Khalid I. Kabel, H. Hassan Ceramics International 38 (2012) 4861–4866.
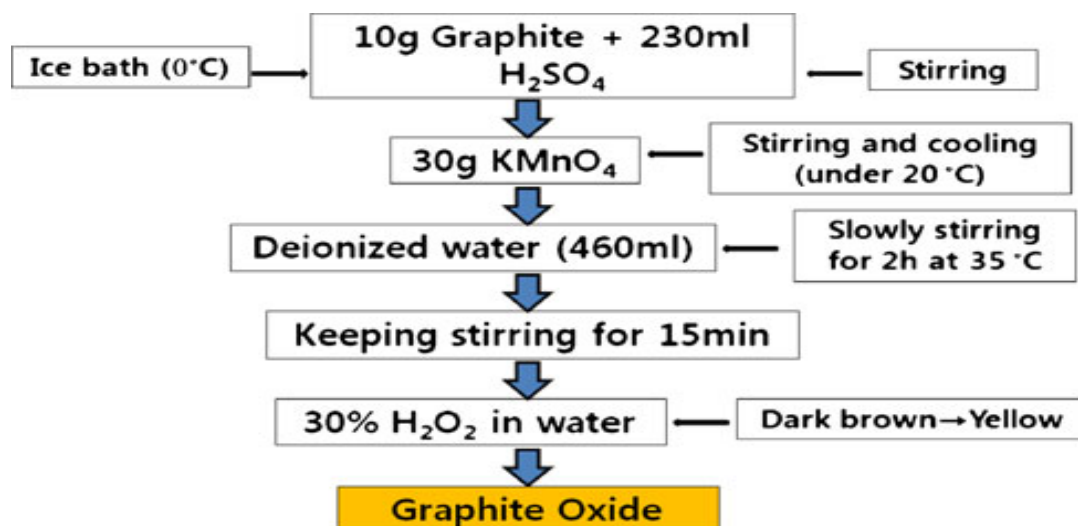
Figure (1): Schematic diagram for synthesis of GO.
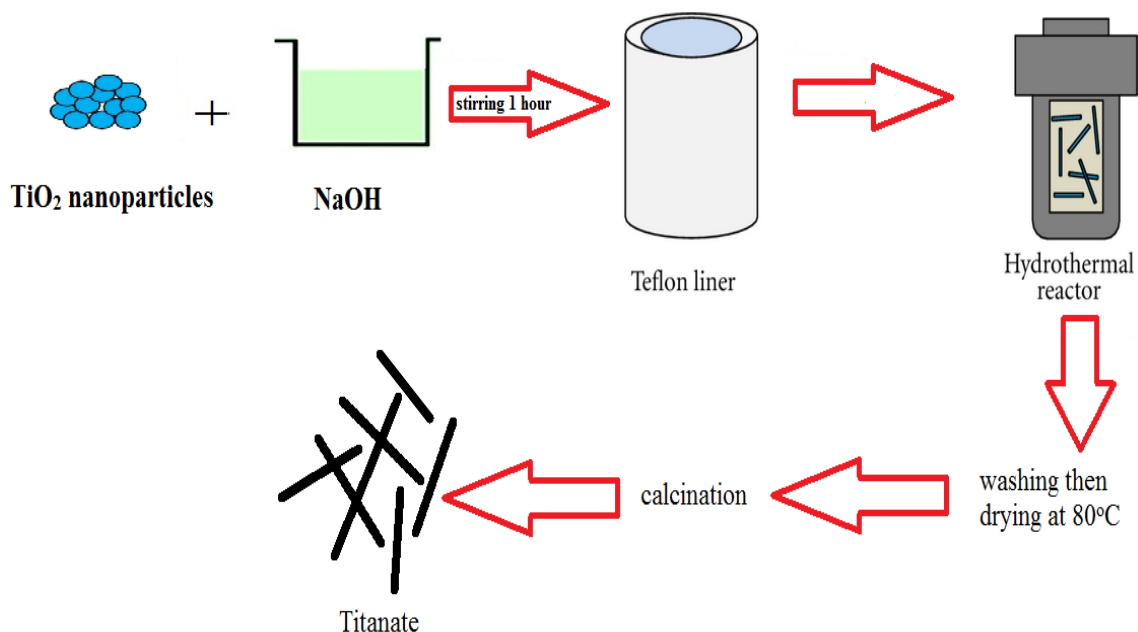
Figure (2): Schematic diagram for TiO₂ nanotubes synthesis.

Military Technical College
Kobry El-Kobbah,
Cairo, Egypt

8ᵗʰ International Conferenc
on
Chemical & Environmenta
Engineering
19 – 21 April 2016
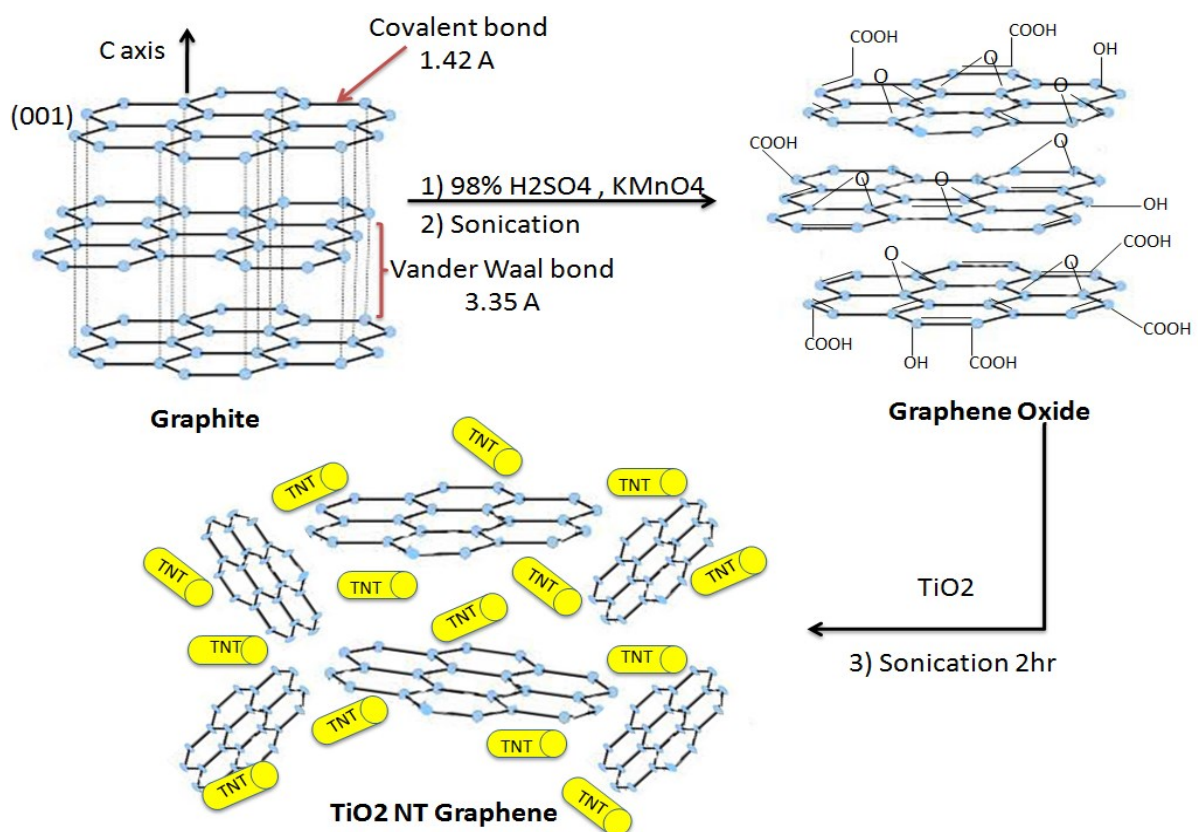
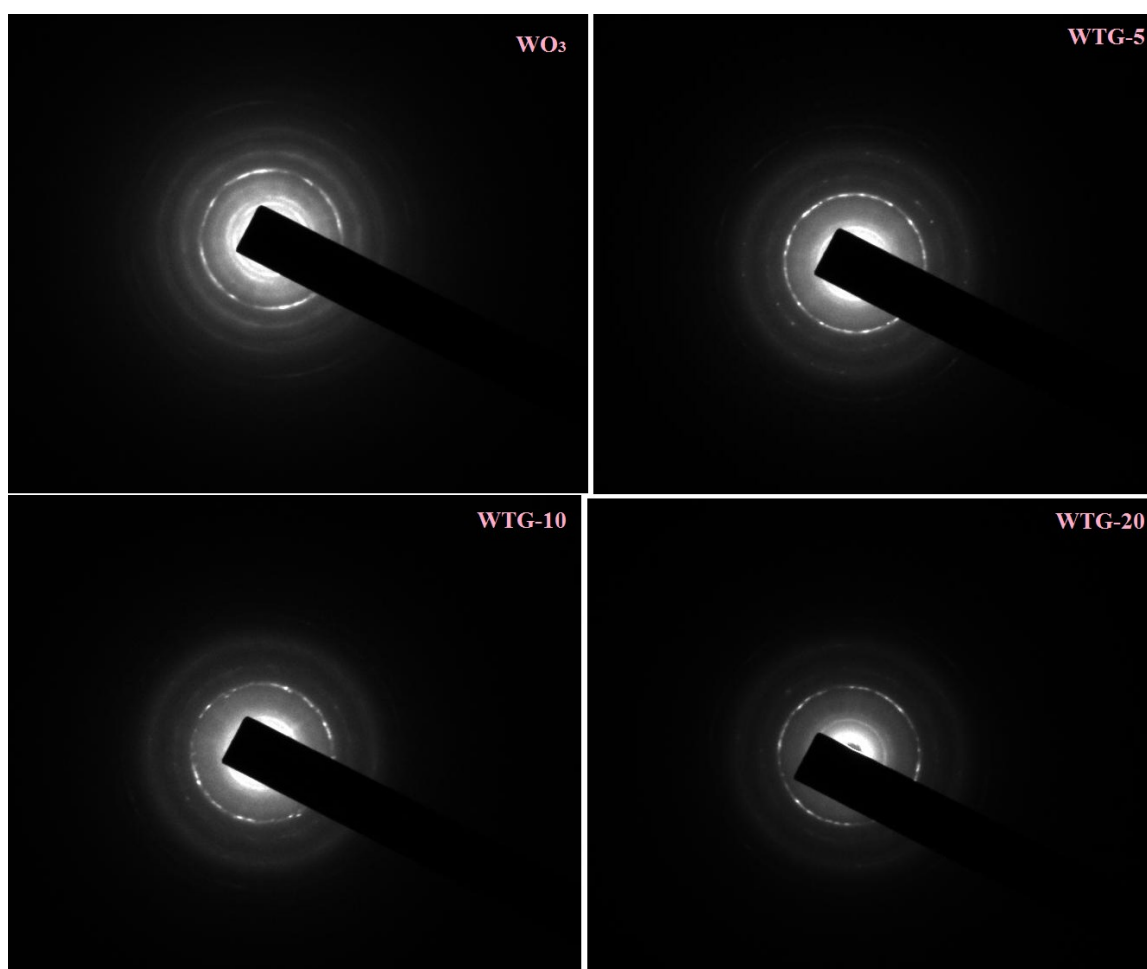
Figure (3): The synthetic route of TG
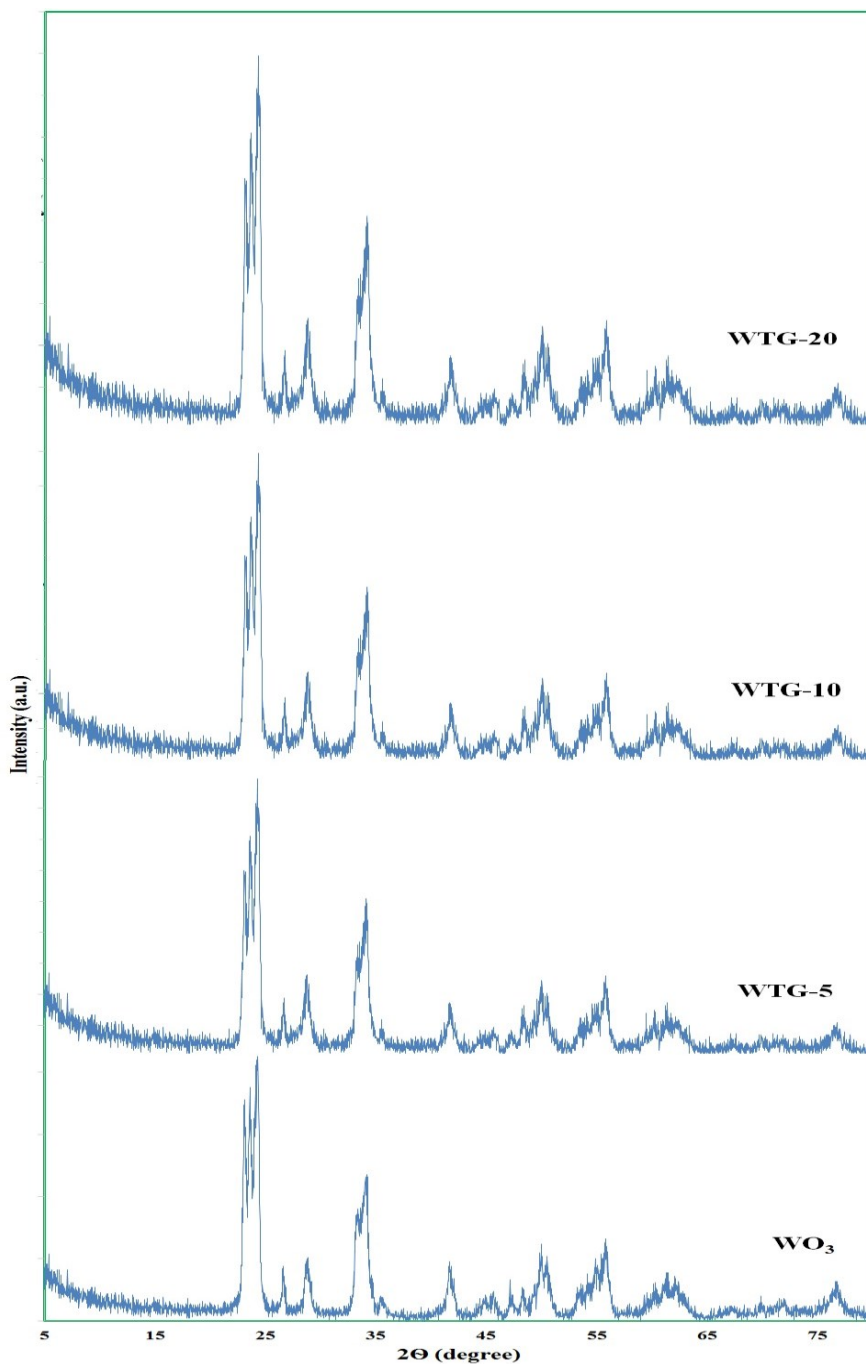
Figure (4): XRD patterns of WO3 and WTGs ternary nanocomposites.

Military Technical College
Kobry El-Kobbah,
Cairo, Egypt

8ᵗʰ International Conferenc
on
Chemical & Environmenta
Engineering
19 – 21 April 2016
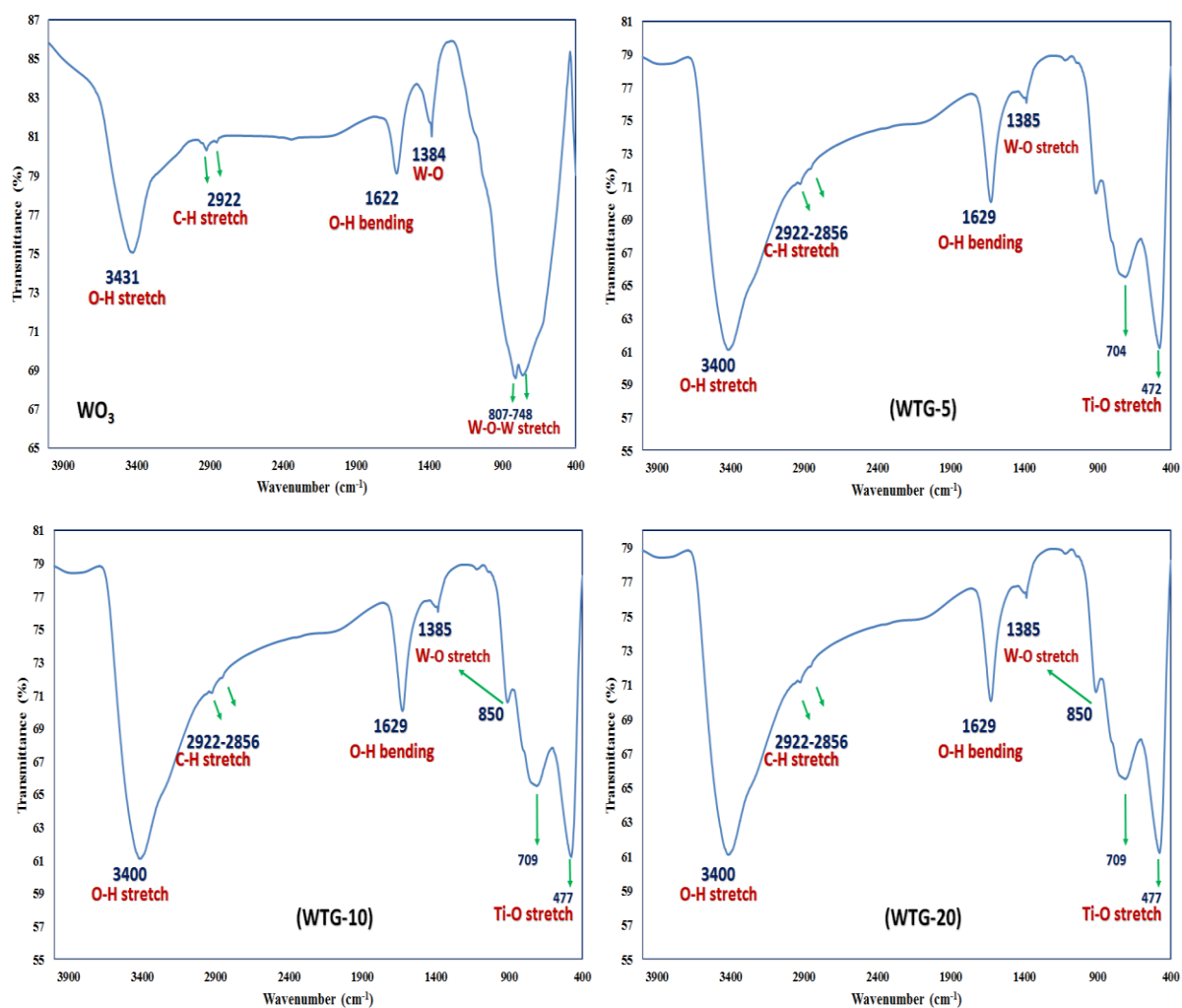
Figure (5) FTIR curves of WO₃ and WTGs ternary nanocomposites.
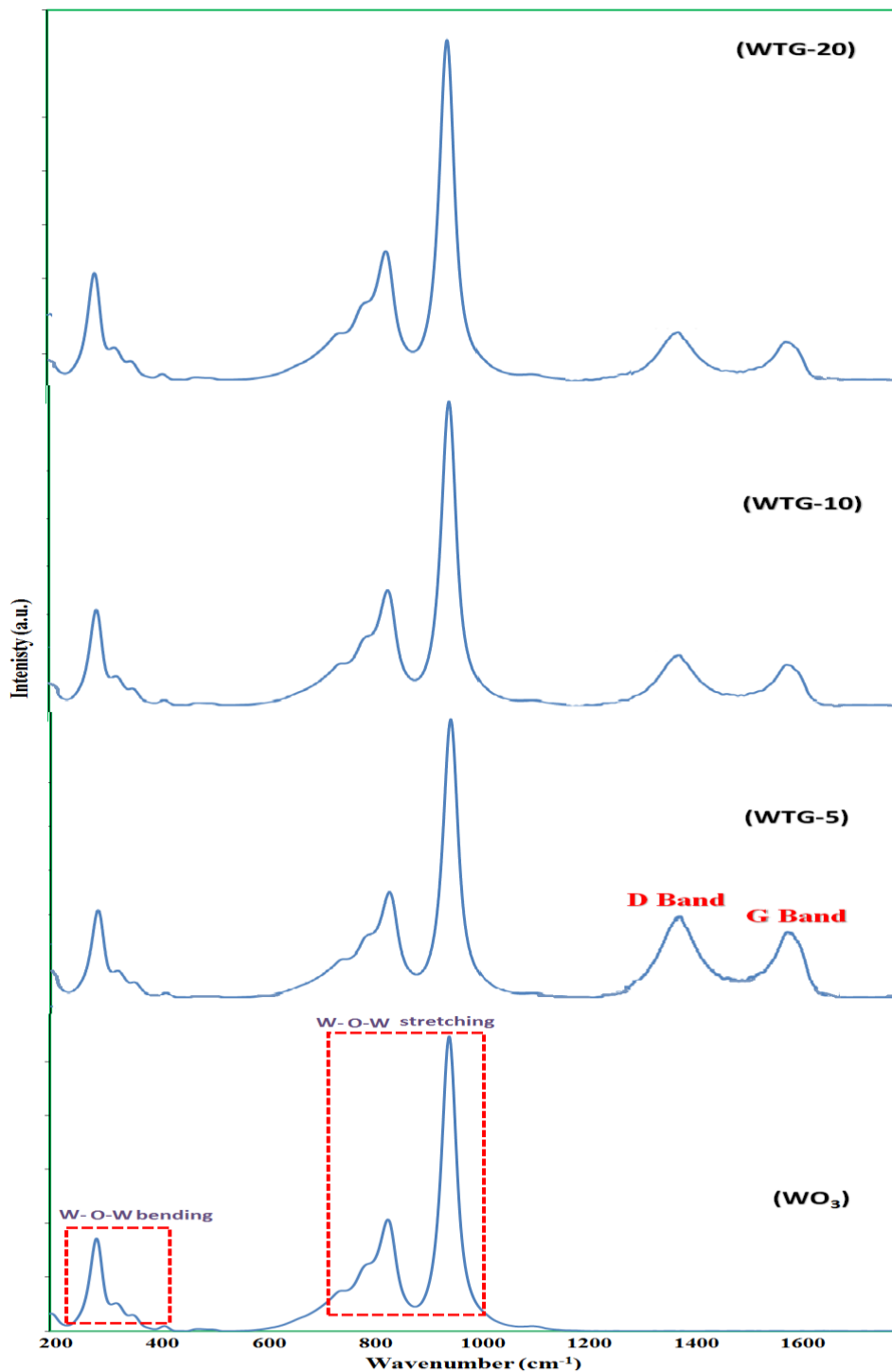
Figure (6) Raman spectra of WO₃ and WTGs ternary.

Military Technical College
Kobry El-Kobbah,
Cairo, Egypt

8th International Conferenc
on
Chemical & Environmenta
Engineering
19 – 21 April 2016
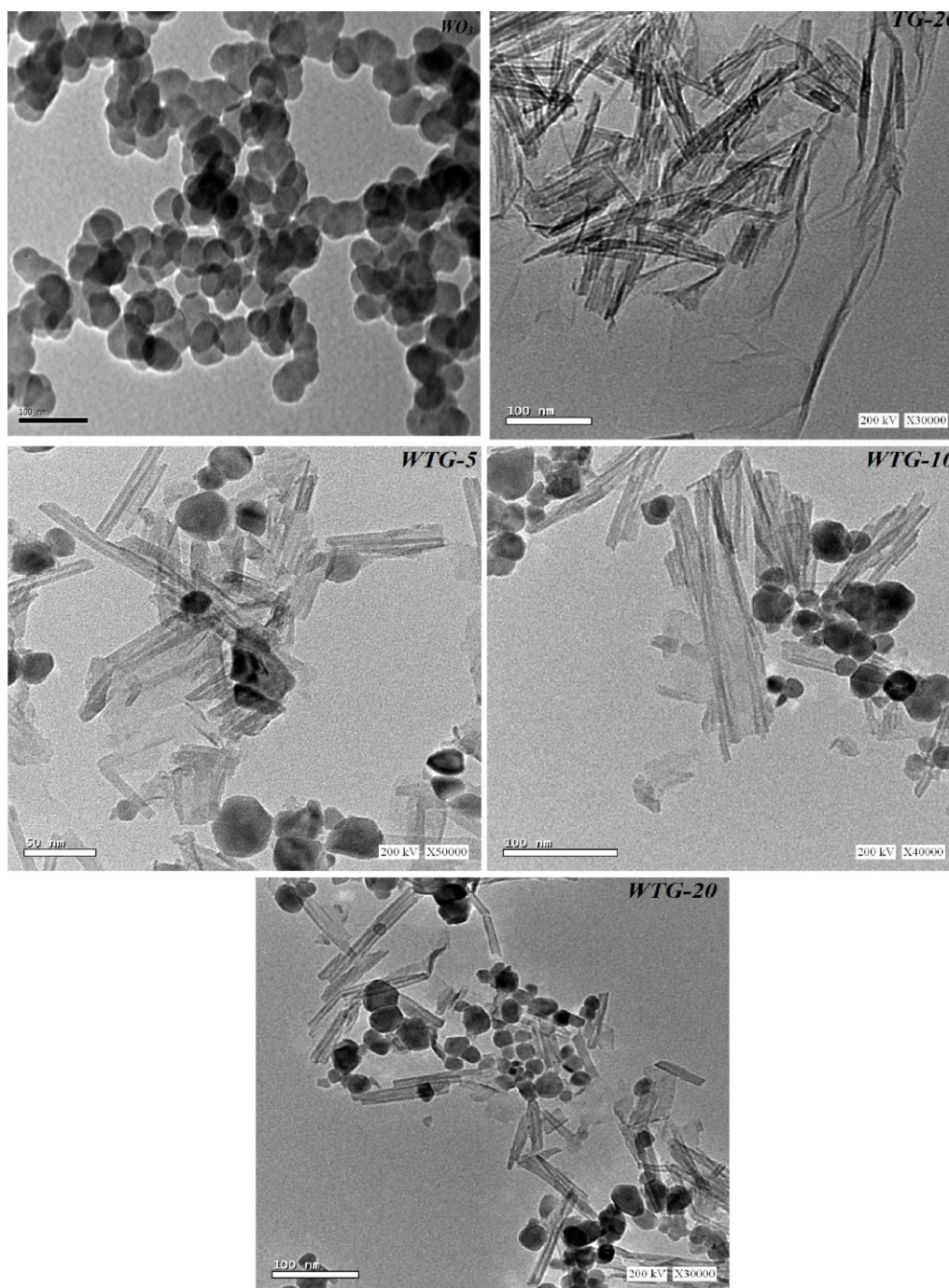
Figure (7) HR-TEM images of WO$_3$ and WTGs ternary nanocomposites.

Figure (8) SAED patterns of WO_3 and WTGs ternary nanocomposites.
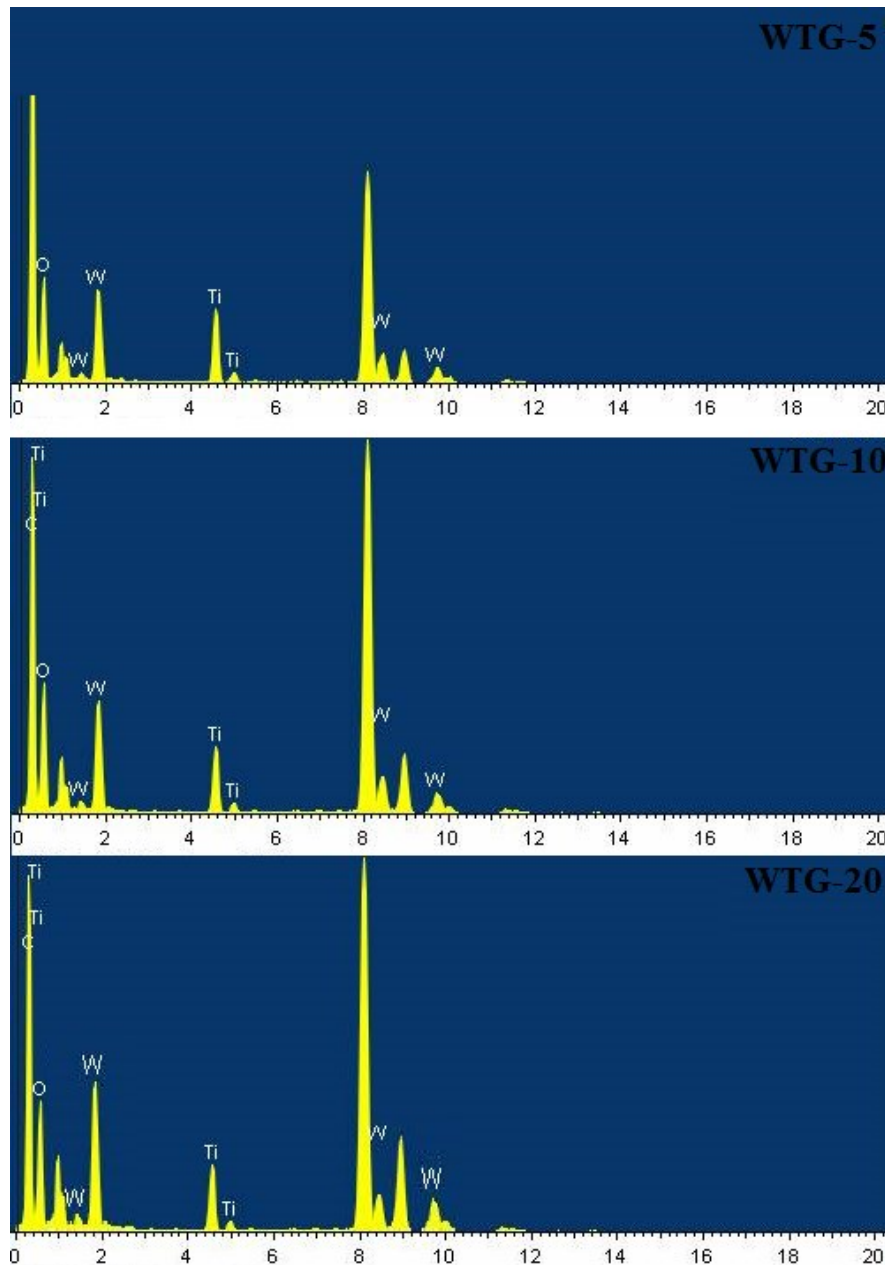
Figure (9) The Energy-Dispersive X-ray (EDX) of WTGs ternary nanocomposites.

Military Technical College
Kobry El-Kobbah,
Cairo, Egypt

**8ᵗʰ International Conference
on
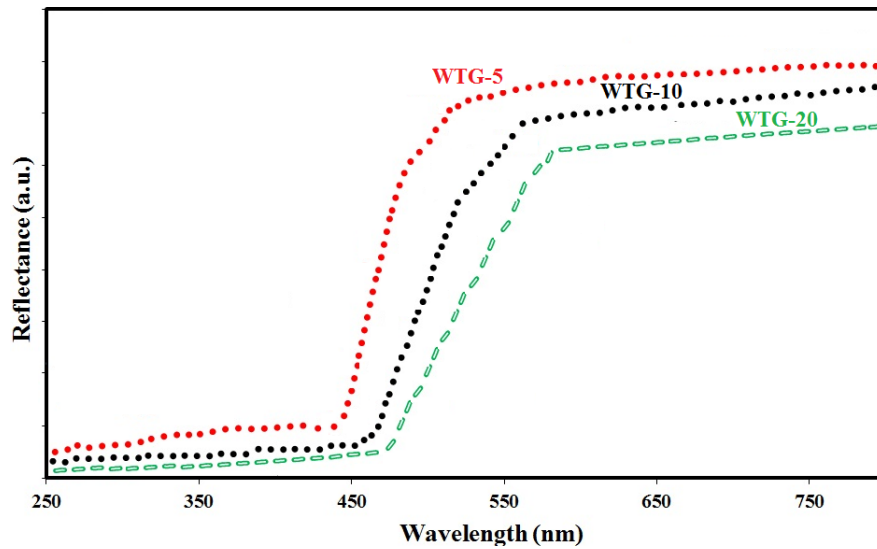Chemical & Environmental
Engineering**
19 – 21 April 2016

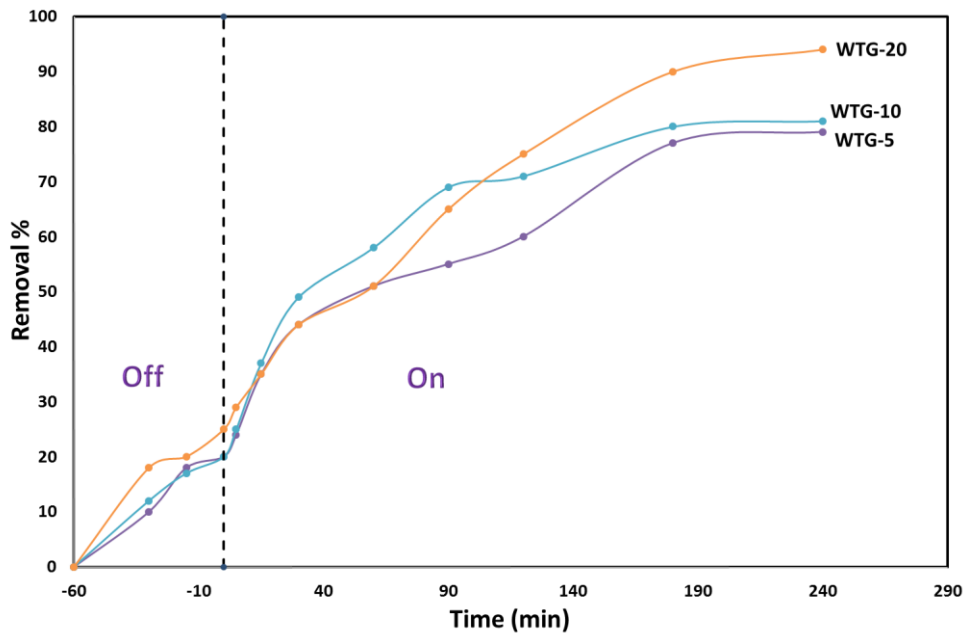**Figure (10) UV– vis diffuse reflectance of WTGs nanocomposites.**

Figure (11) The adsorption and solar photocatalytic degradation of phenol over the WTGs nanocomposites.

Figure (12) An illustration of the Schottky junction between TG/WO$_3$.